ELSEVIER

Biochimica et Biophysica Acta 1419 (1999) 229–247

BIOCHIMICA ET BIOPHYSICA ACTA
BBA

www.elsevier.com/locate/bba

Phase diagram of 1,2-dioleoylphosphatidylethanolamine (DOPE):water system at subzero temperatures and at low water contents

Evgenyi Y. Shalaev *, Peter L. Steponkus

Department of Soil, Crop and Atmospheric Sciences, Cornell University, Ithaca, NY 14853, USA

Received 18 March 1999; accepted 16 April 1999

Abstract

The phase behavior of partially hydrated 1,2-dioleoylphosphatidylethanolamine (DOPE) has been studied using differential scanning calorimetry and X-ray diffraction methods together with water sorption isotherms. DOPE liposomes were dehydrated in the H_{II} phase at 29°C and in the L_α phase at 0°C by vapor phase equilibration over saturated salt solutions. Other samples were prepared by hydration of dried DOPE by vapor phase equilibration at 29°C and 0°C. Five lipid phases (lamellar liquid crystalline, L_α; lamellar gel, L_β; inverted hexagonal, H_{II}; inverted ribbon, P_δ; and lamellar crystalline, L_c) and the ice phase were observed depending on the water content and temperature. The ice phase did not form in DOPE suspensions containing < 9 wt% water. The L_c phase was observed in samples with a water content of 2–6 wt% that were annealed at 0°C for 2 or more days. The L_c phase melted at 5–20°C producing the H_{II} phase. The P_δ phase was observed at water contents of < 0.5 wt%. The phase diagram, which includes five lipid phases and two water phases (ice and liquid water), has been constructed. The freeze-induced dehydration of DOPE has been described with the aid of the phase diagram.

Keywords: Phosphatidylethanolamine; Differential scanning calorimetry; X-ray diffraction; Phase diagram; Water sorption; Ice melting

1. Introduction

Binary phospholipid:water mixtures have been widely used as models of biological membranes. One of the major areas of interest is the influence of water on lipid mesomorphism, which is essential to a mechanistic understanding of destabilization of biological membranes under severe environmental conditions such as freezing and desiccation [1,2]. To describe the relationships between water content

Abbreviations: PC, phosphatidylcholine; PE, phosphatidylethanolamine; DOPE, 1,2-dioleoyl-*sn*-glycero-3-phosphatidylethanolamine; DDPE, 1,2-didodecyl-*rac*-glycero-3-phosphoethanolamine; DAPE, 1,2-diarachinoyl-*sn*-glycero-3-phosphoethanolamine; POPE, 1-palmitoyl-2-oleoyl-*sn*-glycero-3-phosphoethanolamine; L_α, lamellar liquid crystalline phase; L_β, lamellar gel phase; H_{II}, inverted hexagonal phase; L_c, lamellar crystalline phase; P_δ, inverted ribbon phase; T^i_{m1}, the L_β+ice→L_α+ice invariant phase transition temperature; T^i_{m2}, the L_c+L_β→L_c+H_{II} invariant phase transition temperature; T_m, the L_β+water→L_α+water invariant phase transition temperature in the supercooled samples; T^i_w, the L_α+ice→L_α+water invariant phase transition temperature; T^m_{w1}, the L_α+ice→L_α monovariant phase transition temperature; T^m_m, the L_β→L_β+L_α monovariant phase transition temperature; T^m_{w2}, the L_β+ice→L_β monovariant phase transition temperature; T_{bh}, the temperature of the monovariant L_α→H_{II}+L_α→H_{II} and invariant L_α+water→H_{II}+water phase transitions; T_c, the L_c-to-H_{II} phase transition temperature; Superscripts i and m refer to the invariant and monovariant phase transitions, respectively

* Corresponding author. Present address: Central Research Division, Pfizer Inc., Groton, CT 06340, USA. Fax: +1-860-441-0467; E-mail: evgenyi_y_shalaev@groton.pfizer.com

0005-2736/99/$ – see front matter
PII: S0005-2736(99)00068-1

and lipid phase behavior, phase diagrams are usually used.

Phospholipids can adopt a number of phases, and it complicates study and construction of the phase diagrams. For example, seven phases were described for 1,2-dodecyl-*rac*-glycero-3-phosphoethanolamine [3]. Quite often, certain phase(s) occupy narrow temperature/water content regions, which are very difficult to resolve experimentally. For example, in a DL-dipalmitoylphosphatidylcholine:water system [4] the temperature region of phase coexistence of $P_{\beta}'+L_{\alpha}$ is about 2°C, and the composition range is less than 7 wt% of the water. Moreover, phospholipids often exist in a metastable state rather than in an equilibrium one, which also complicates the study and construction of phase diagrams of phospholipid:water systems. The best known example is the metastability of the gel phase with respect to the lamellar crystalline phase (reviewed in [5]). Despite these problems, phase diagrams have been constructed for several saturated species of PC and PE [6]. Phase diagrams for unsaturated species of phospholipids have been studied to a much lesser extent, even though unsaturated phospholipids are the predominant phospholipid species in biological membranes.

In this report, the phase diagram of a DOPE:water system has been studied. DOPE is the most studied species of PE with unsaturated hydrocarbon chains and has been used as a model to study the influence of different solutes on lipid phase transitions [7] and (in mixtures with other lipids) to study freeze-induced destabilization of biological membranes [8–10]. Phase transitions in DOPE at water contents above 5 wt% and temperatures above 0°C have been studied in some detail [8,11–14]. In particular, the part of the phase diagram that includes two lipid phases (L_{α} and H_{II}) and a liquid water phase has been constructed [11,15]. Two other phases, the cubic [14] and inverted ribbon [16] phases, have also been reported to exist. In the present study, the phase behavior of partially hydrated DOPE has been studied using differential scanning calorimetry (DSC) and X-ray diffraction methods together with water sorption isotherms. Major attention has been devoted to the low-temperature (below 0°C) and low-water content (below 5 wt%) regions for which only fragmentary data are reported in the literature. Water sorption isotherms for DOPE in the L_{α} phase at 0°C and in the H_{II} phase at 29°C were obtained, and DOPE samples with water contents from 0 to 25 wt% were analyzed by DSC and small- and wide-angle X-ray diffraction. The phase diagram that describes phase equilibria involving five lipid phases and two water phases (ice and liquid water) has been constructed. An example of how a phase diagram of a phospholipid:water system can be used in cryobiology is provided in Section 4. One of the important cryobiological issues is the freeze-induced dehydration of lipid bilayers [17]. The hydration of DOPE in the presence of the ice and liquid water phase as a function of temperature below 0°C has been estimated, and freeze-induced dehydration of DOPE has been described with the aid of the phase diagram.

2. Materials and methods

2.1. Sample preparation

DOPE was purchased from Avanti Polar Lipids as a chloroform solution and used without further purification. Chloroform was removed under a stream of N_2 at room temperature followed by drying under vacuum for at least 15 h. DOPE liposomes were prepared in double-distilled, de-ionized water saturated with N_2 by freeze-thaw cycling in liquid nitrogen and a water bath at 1–3°C with vortexing between cycles; ten freeze-thaw cycles were employed. Lipid concentration was 100–200 mg lipid/ml water.

Partially hydrated DOPE samples for X-ray and DSC experiments were prepared by dehydration of the DOPE liposomes as well as hydration of dried lipid by vapor phase equilibration. Equilibration was performed at two temperatures: at 29.0 ± 0.5°C in an incubator, and at 0.5 ± 1.5°C in a cold room (referred to as equilibration at 0°C). During equilibration in the cold room, containers with DOPE were kept in an ice/water mixture. To prepare the DSC samples, DSC pans containing either DOPE liposomes or dried DOPE were placed over pure water or saturated salt solutions in tightly closed jars; the jars were flushed with argon, and DOPE was equilibrated for 6–10 days at 29°C and 19–25 days at 0°C. After equilibration, the DSC pans were sealed hermeti-

cally. To prepare samples for X-ray diffraction experiments, Petri dishes containing DOPE liposomes or dried DOPE were placed over saturated salt solutions in desiccators; the desiccators were evacuated with a vacuum pump and stored at either 29°C or 0°C for 6–10 days. After equilibration, the DOPE samples were loaded into X-ray capillaries and further equilibrated over saturated salt solutions for an additional day after which the capillaries were flame-sealed. All operations with samples equilibrated at 0°C were performed in a cold room at 2–4°C using cooled tweezers; relative humidity (RH) in the cold room was 60–70%. Samples equilibrated at 29°C were transferred into capillaries at room temperature at RH 30–40%. It appeared that a number of samples lost a considerable amount of water during loading. To account for such uncontrolled dehydration, the water content of the samples was determined after the X-ray diffraction experiments as described below.

Saturated aqueous solutions of Na_2HPO_4, KNO_3, $BaCl_2$, KCl, NaCl, NaBr, $MgCl_2$, and LiCl were used to control DOPE hydration [8]. Corresponding osmotic pressures, Π, for those solutions were calculated at 30°C and 0°C as described in [18]

$$\Pi = -(RT/V_w)\ln(RH/100) \quad (1)$$

where $R = 8.31$ J mol^{-1} K^{-1} is the universal gas constant, T is temperature in K, V_w is the partial molar volume of water in the solution, RH is the relative humidity of the solution. Partial molar volumes of water in the solutions were calculated from the density-concentration dependence as described by [18] using densities given in [19]. However, the molar volume for pure water may be used because it appeared that the difference between partial molar volume of water in pure water and in the solutions under consideration is negligible. RH values and osmotic pressures for the saturated salt solutions used in this study are given in Table 1.

Water content was determined gravimetrically after DSC and X-ray diffraction experiments by drying lipids in DSC pans with pin holes at 70°C under vacuum until a constant weight was achieved (usually 3.5 h).

2.2. DSC and X-ray diffraction experiments

DSC experiments were performed with a Perkin-Elmer DSC-7 instrument. The instrument was calibrated using melting points of water and indium at a heating rate of 10°C/min. An empty aluminum pan was used as a reference. Samples were cooled to either −10 to −20°C (to avoid ice formation) or −120 to −140°C followed by immediate heating to 30–35°C; cooling and heating cycles were repeated several times. DSC pans usually contained 1–2 mg of lipid. Samples equilibrated at 0°C were transferred into the pre-cooled DSC instrument at 0°C. Heating and cooling rates were usually 40°C/min. At this high heating rate, the apparent melting temperatures of water and indium were (1.1 ± 0.5)°C higher than those obtained at 10°C/min; the values for the phase transition temperatures reported in this study were corrected for the difference. Some samples were also scanned at lower scanning rates (5, 10, and 20°C/min) to ensure that the high scanning rates did not cause major changes in the phase behavior

Table 1
Relative humidities and osmotic pressures of saturated salt solutions

Saturated aqueous solution of	30°C		0°C	
	osmotic pressure, MPa	RH, %	osmotic pressure, MPa	RH, %
Na_2HPO_4	4.3	97 [20]	2.5	98[a]
KNO_3	11.2	92.3 [21]	4.8	96.3 [21]
$BaCl_2$	16.3	89 [20]	7.8	94[a]
KCl	25.1	83.6 [21]	15.3	88.6 [21]
NaCl	40.1	75.1 [21]	35.4	75.5 [21]
NaBr	81.1	56.0 [21]	57.3	63.5 [21]
$MgCl_2$	157.7	32.4 [21]	137.2	33.7 [21]
LiCl	305.2	11.3 [21]	276.1	11.2 [21]

[a]Extrapolated from 5°C to 0°C using data from [20].

of the DOPE. The more rapid heating rates did not cause changes in the general appearance of the DSC curves.

X-ray diffraction powder patterns were obtained at the Cornell High Energy Synchrotron Source (CHESS) using the D1 station. Wavelength was measured using silver benhamate and was 0.70 Å and 0.93 Å in different experiments. Diffraction patterns were recorded on Polaroid film placed at a measured specimen-to-film distance. Sample temperature was maintained using an air-jet cooling system and measured by a thermocouple placed in the air stream close to the capillary. The difference between the sample temperature and the thermocouple temperature was estimated to be less than 5°C. Samples equilibrated at 29°C were loaded in the X-ray diffraction instrument at room temperature (~20°C), and cooled to −40 to −50°C at a rate of ~15°C/min. Samples equilibrated at 0°C were transferred to X-ray diffraction facilities at 0°C and placed into a pre-cooled sample holder at −40°C. X-ray diffraction patterns were obtained at several temperatures between −50 and 30°C. The intermediate temperatures for measurements were chosen to be below and above the temperature of thermotropic events on DSC curves and were usually −20 to −15°C and 0–10°C. In several instances, the cooling-heating cycle was repeated to ensure reversibility. Samples were equilibrated at every temperature for at least 5 min before the X-ray diffraction patterns were collected.

3. Results

3.1. X-ray diffraction studies

3.1.1. Fully hydrated DOPE

Repeat spacings for the fully hydrated DOPE were consistent with those reported in the literature [22]; the repeat spacings were 5.6 nm (at temperatures between −40 and −15°C), 5.3 nm (from −0.5 to 10°C) and 6.9 nm at 10°C for the L_β, L_α, and H_{II} phases, respectively. Coexistence of the L_β and the ice phase was observed between −50 and −4°C; the L_α phase was observed at 0°C; coexistence of the L_α and H_{II} phases was observed at 10°C; and the H_{II} phase alone was observed at 25°C.

3.1.2. Partially hydrated DOPE. Equilibration at 29°C

DOPE samples, which contained 0.2–20 wt% water, were prepared by dehydration of fully hydrated DOPE liposomes at 16–158 MPa, and hydration of dried DOPE at 4–81 MPa by vapor phase equilibration at 29°C. Four lipid phases (L_α, L_β, H_{II}, and P_δ phase) and the ice phase were observed depending on the water content and temperature.

At 30°C and a water content ranging from 4 to 20 wt%, several small-angle reflections indexing to ratios of $1:\sqrt{3}:\sqrt{4}:\sqrt{7}$ were observed, which allowed us to identify this phase as the H_{II} phase. At a water content of 11–20 wt% and −50 to −10°C, 2–4 small-angle reflections indexing to ratios of 1:2:3:4, which is characteristic of the lamellar phase, were observed. In the wide angle patterns, several reflections were observed; a reflection at (0.445 ± 0.005) nm was assigned to the L_β phase, and reflections with $d = (0.19 \pm 0.01)$, 0.26, 0.33, (0.355 ± 0.005), 0.38 nm were assigned to the ice phase. For comparison, data for ice that are reported in the literature are as follows: 0.192, 0.207, 0.267, 0.344, 0.367, 0.390 nm [23]. Hence, in those samples the L_β and ice phases coexisted. A diffraction ring with a *d*-spacing of (0.23 ± 0.01) nm that did not match the ice pattern was also observed in these samples; the origin of this diffraction ring is obscure. In samples with a water content of 4–9 wt%, only the L_β phase was observed between −50 and −10°C; the ice phase was not observed.

At 0–10°C and a water content >9 wt%, the L_α phase alone or in coexistence with the H_{II} phase was observed. The L_α phase was identified as having several small-angle reflections indexing 1:2:3 and a broad wide-angle reflection centered at 0.43 nm. Note that in one of the samples (water content 18.7 wt%) that was cooled to −40°C and then heated to 30°C, coexistence of the L_α and H_{II} phases was observed even at temperatures as high as 30°C; however, the L_α phase disappeared when the sample was held for several h at room temperature. This observation indicates that the $L_\alpha \rightarrow H_{II}$ transition is a slow process and may require several hours to be completed. Slow kinetics of the $L_\alpha \rightarrow H_{II}$ phase transition has been reported for fully hydrated DOPE [24].

At water contents less than 0.5 wt%, two small-angle reflections (a first-order reflection at 3.93 nm)

and one sharp reflection at 0.37 nm and a broad reflection centered at 0.44 nm in the wide-angle region were observed (Fig. 1). The ratio of small-angle *d*-spacings (1:1.86) indicates that this is neither the lamellar, hexagonal, nor cubic phase. We identified this phase as an inverted ribbon phase, P_δ, after Pohle and Selle [16]. Using infra-red spectroscopy, Pohle and Selle [16] have shown that DOPE equilibrated at $RH \leq 50\%$ enters the ribbon phase; they also suggested that this is a phase with largely disordered hydrocarbon tails. However, the existence of a sharp reflection in the wide-angle region observed in this study (Fig. 1B) does not support the suggestion about disordered hydrocarbon chains; instead this observation indicates some (partial) order.

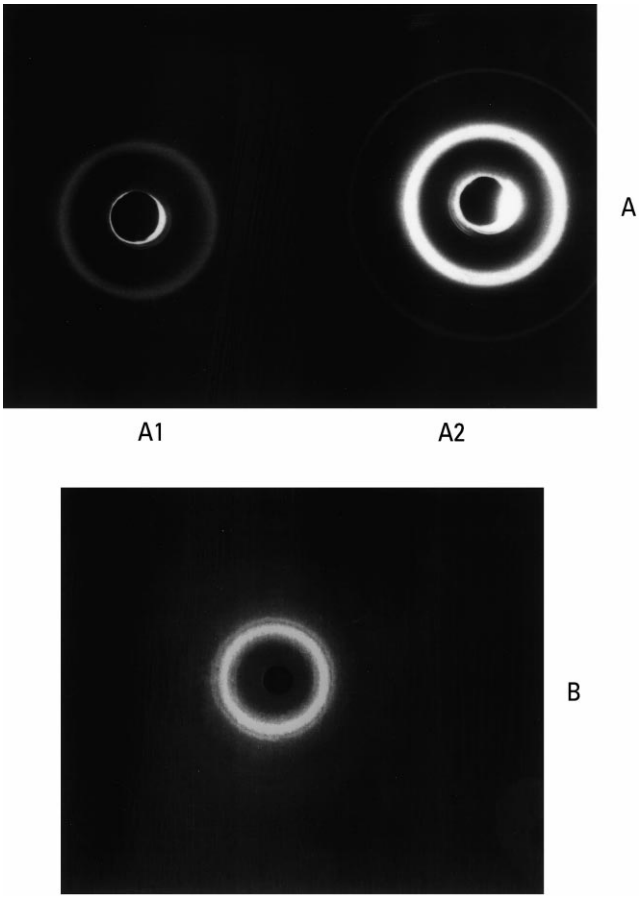

Fig. 1. Representative small-angle and wide-angle X-ray diffraction patterns of the P_δ phase at 30°C; wavelength was 0.93 Å. (A) Small-angle patterns at different exposure times; sample-to-film distance was 392 mm, exposure time 60 s (A1) and 300 s (A2). (B) Wide-angle pattern; sample-to-film distance was 31 mm.

The inverted cubic phase of DOPE has been reported to exist at certain conditions [11,14]. However, the cubic phase was not detected in this work. There are two possible reasons as follows: (i) difference in the thermal history in [14] (ten thermocycles were employed) and in this work; (ii) very narrow temperature/composition range of existence of the inverted cubic phase; the cubic phase was observed in a sample with 11 wt% water at 1–12°C, and was not observed in samples with ~8 and ~15 wt% water [11].

Phases that were observed at different water contents and temperatures are given in Table 2. X-ray diffraction data show that during equilibration at 29°C at different osmotic pressures, DOPE exists in the H_{II} phase at water contents >3 wt%, and in the P_δ phase at water contents close to zero. Ice formation was observed in samples with water contents ≥ 11 wt% but not at water contents <9 wt%.

3.1.3. Partially hydrated DOPE. Equilibration at 0°C

DOPE liposomes were dehydrated from the fully hydrated state at 8 and 35 MPa at 0°C; dried DOPE was hydrated through vapor phase equilibration at 8, 15, and 35 MPa. X-ray diffraction patterns for all of these samples were similar. Water content was 3.3–4.9 wt% which is lower than in DSC samples equilibrated at 8 and 15 MPa in DSC pans; the difference is most likely due to loss of water during loading of capillaries. Representative X-ray diffraction patterns obtained at −40°C are shown in Fig. 2. Several small-angle reflections with ratio 1:2:3 (first-order reflection at 5.10–5.33 nm) were observed. Wide-angle reflections at 0.33, 0.39, 0.44 nm, and several faint, poorly resolved reflections with higher *d*-spacing were observed indicating a highly ordered three-dimensional structure. This phase was identified as the lamellar crystalline phase, L_c. A weak small-angle diffraction ring with a *d*-spacing of 5.59–5.87 nm was also observed in several samples (not shown) that is assigned to minor L_β phase, which coexists with the L_c phase. The X-ray diffraction patterns (both small and wide angle) did not change during heating from −40 to −15°C. At 5°C, the *d*-spacing of the minor small-angle ring decreased from (5.75 ± 0.15) nm to (4.65 ± 0.25) nm indicative of a phase transition from the L_β to another phase. This phase was provisionally identified as the

H_{II} phase because the repeat spacing was similar to that which was observed for the H_{II} phase at a corresponding water content. At 15°C, the *d*-spacing corresponding to the minor ring decreased to (4.05 ± 0.15) nm. The decrease in the *d*-spacing is likely to be associated with the temperature dependence of *d*-spacing for the H_{II} phase. The wide-angle patterns did not change during heating from −40 to 15°C indicating coexistence of the major L_c phase together with the minor L_β phase (at −40 to −15°C) or the H_{II} phase (at 5–15°C). At 25°C, the sharp, wide-angle reflections disappeared; in the small-angle region, one first-order reflection with $d = (3.95 \pm 0.25)$ nm was observed and was assigned to the H_{II} phase. Cooling to −25°C did not restore the original X-ray diffraction patterns; instead, one wide-angle reflection at (0.405 ± 0.005) nm and two or more small-angle reflections (1:2:3:4 ratio, repeat spacing varied from 5.10 to 5.59 nm in different samples) were observed and allowed us to identify this phase as the L_β phase. When the heated samples were annealed at 0°C for at least 2 days, the L_c phase was observed again. A summary of the X-ray diffraction results is given in Table 2.

The occurrence of the L_c phase in a DOPE:water system has not been previously reported in the literature. Two lamellar crystalline phases (L_{c1} and L_{c2}) were observed in DOPE that was hydrated with DMSO:water mixtures at DMSO concentrations greater than 50% [22]. The X-ray diffraction patterns (both wide-angle and small-angle) for the L_{c2} phase [22] have some similarities with the L_c phase in this study; however, the correspondence is not perfect, and it is not clear whether the two phases (the L_c phase in this study and the L_{c2} phase reported in [22]) are identical.

3.2. DSC results

3.2.1. Fully hydrated DOPE

In DSC heating curves of fully hydrated DOPE (not shown), two endothermic peaks, T_m and T_{bh}, corresponding to the L_β-to-L_α (stronger peak) and L_α-to-H_{II} (weaker peak) phase transitions, were observed when the sample was scanned between −12 and 30°C. When the samples were cooled to −140°C, the T_m peak (L_β-to-L_α phase transition) was followed by a large ice melting peak. The temperatures and enthalpies for the phase transitions of fully hydrated DOPE obtained at different heating rates are given in Table 3, which also contains the data from the literature for comparison. There is reasonable

Table 2
X-ray diffraction results for partially hydrated DOPE samples at different temperatures

Water content, wt%	Temperature, °C										
	−45...−30	−20	−15	−10	0	5	10	20	30	−40 (after 25°C)	−40 (2 days at 0°C)
18.9[a]	L_β+ice	–	–	L_β+ice	–	L_α	L_α+H_{II}	–	H_{II}	–	–
13.2[a]	L_β+ice	–	–	–	–	–	–	H_{II}	–	–	–
11.6[a]	–	L_β+ice	–	–	–	L_α	–	–	H_{II}	–	–
10.7[a]	L_β+ice	L_β+ice	–	–	L_α	–	–	H_{II}	H_{II} (35°C)	–	–
8.8[a]	L_β	L_β	–	–	L_α+H_{II}	–	H_{II}	–	H_{II}	–	–
6.5[a]	L_β	–	L_β	–	–	–	H_{II}	–	H_{II}	–	–
4.2[a]	L_β	–	L_β+H_{II}	–	–	–	H_{II}	–	H_{II}	–	–
2.8–3.1[a]	L_β	–	L_β	–	–	–	H_{II}	–	H_{II}	–	–
0.2–0.4[a]	P_δ	–	–	–	–	–	–	–	P_δ (up to 50°C)	–	–
3.3–4.9[b]	L_c or L_c+L_β	–	L_c or L_c+L_β	–	–	L_c or L_c+ H_{II}	L_c+ H_{II} or H_{II} (15°C)	–	H_{II} (25°C)	L_β	L_c or L_c+L_β

[a]The samples were prepared by dehydration of DOPE liposomes and hydration of dried DOPE through vapor phase equilibration at 29°C.

[b]The samples were prepared by dehydration of DOPE liposomes and hydration of dried DOPE through vapor phase equilibration at 0°C.

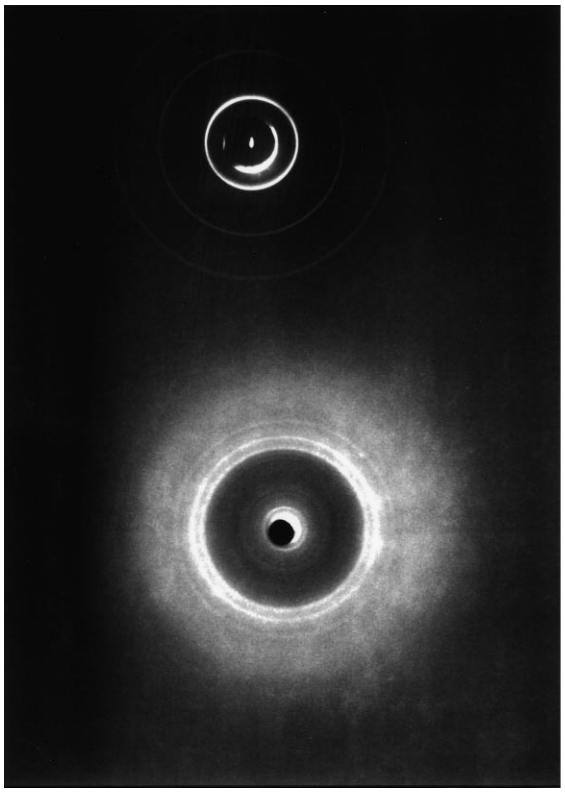

Fig. 2. Representative small-angle and wide-angle X-ray diffraction patterns of the L_c phase at −40°C; wavelength was 0.70 Å. (A) Small-angle pattern; sample-to-film distance 419 mm, exposure time 55 s. (B) Wide-angle pattern; sample-to-film distance 60 mm, exposure time 13 s.

agreement between the data from this study and the literature.

3.2.2. Partially hydrated DOPE. 0°C equilibration

Representative DSC heating curves of DOPE liposomes that were dehydrated in the L_α phase at different osmotic pressures at 0°C are shown in Fig. 3. The general appearance of the DSC curves and their reversibility depends on the hydration. For samples that were equilibrated at 0–15 MPa (water content ≥11 wt%, Fig. 3, curves a–f), the DSC heating curves were completely reversible, i.e. there was no difference between the first and successive scans. One or two major endothermic peaks below 0°C followed by a weak endothermic peak were observed on the DSC heating curves for those samples. The weak endothermic peak above 0°C, T_{bh}, is assigned to the L_α-to-H_{II} phase transition of DOPE. The number and/or magnitude of the major endothermic peaks that were observed at lower temperatures (around 0°C and lower) were dependent on whether the samples were cooled to −15 to −20°C or −140°C, whereas the T_{bh} was essentially independent of the cooling temperature. If the samples were scanned between −15 and 30°C (Fig. 3, broken curves), water did not crystallize and remained in the supercooled state. In this case, one major endothermic peak slightly below 0°C was observed and is the result of the $L_\beta \rightarrow L_\alpha$ phase transition. If the heating scans were performed from −140°C (Fig. 3, solid curves), the

Table 3
Temperatures and enthalpies of the $L_\beta \rightarrow L_\alpha$ and $L_\alpha \rightarrow H_{II}$ phase transitions of fully hydrated DOPE determined by DSC

Phase transition		This work, at heating rate				Literature data
		40°C/min	20°C/min	10°C/min	5°C/min	
L_β+ice → L_α+ice	T_m	−2.9 ± 0.8°C (peak)	–	−3.3 ± 0.7°C (peak)	–	−8.1°C[c] [8]
		−5.1 ± 0.6°C (onset)	–	−5.4 ± 1.3°C (onset)	–	
	ΔH	–[a]	–	–[a]	–	31.7 kJ/mol[c] [8]
L_β+water → L_α+ water (supercooled)	T_m	−5.5 ± 0.5°C (peak)	−7.8 ± 0.2°C (peak)	−8.6 ± 0.2°C (peak)	−8.8°C (peak)	−7.3 ± 3.8°C[c] [41]
		–[b]	−9.1 ± 0.2°C (onset)	−9.8 ± 0.2°C (onset)	−9.9°C (onset)	
	ΔH	–[b]	23.9 kJ/mol	24.0 kJ/mol	23.6 kJ/mol	18.9 kJ/mol[c] [41]
L_α+water → H_{II}+ water	T_{bh}	19.1 ± 1.8°C (peak)	15.5 ± 1.3°C (peak)	14.9 ± 2.1°C (peak)	13.4°C (peak)	8.5 ± 1.9°C [41]
		15.9 ± 2.2°C (onset)	12.8 ± 2.0°C (onset)	12.7 ± 3.0°C (onset)	11.7°C (onset)	
	ΔH	1.48 ± 0.05 kJ/mol	1.54 kJ/mol	1.34 kJ/mol	1.44 kJ/mol	1.22 ± 0.17 kJ/mol [42]

[a] ΔH was not determined because the T_m peak was not fully resolved from the ice melting peak.
[b] The onset temperature was not determined because the onset temperature was close to the cooling temperature.
[c] It has not been specified whether this transition is in the presence of ice or liquid water. In the description of experimental procedure [8], DSC scans were performed from −40°C; it is most likely that the ice formed at those conditions, and the values reported in [8] are for the phase transition in the presence of ice.

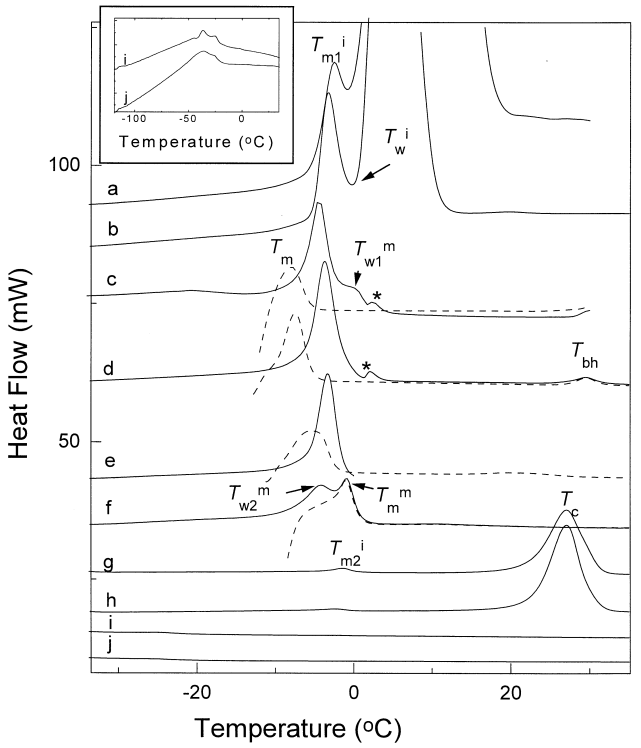

Fig. 3. Representative DSC heating curves of DOPE liposomes dehydrated at 0°C through vapor phase equilibration. Heating rates: 40°C/min. Dotted curves: DSC runs that were performed from −15 to −20°C. Solid curves: scans were performed from −140°C. (a) Fully hydrated; (b) equilibrated at 0 MPa (over pure water); (c) equilibrated at 2.5 MPa, 17.0 wt% water; (d) 4 MPa, 15.8 wt% water; (e) 8 MPa, 13.3 wt% water; (f) 15 MPa, 11.3 wt% water; (g) 35 MPa, 3.0 wt% water; (h) 57 MPa, 2.4 wt% water; (i) 137 MPa; (j) 276 MPa. Inset: DSC heating curves of DOPE dehydrated at 137 and 276 MPa.

sub-zero parts of the DSC heating curves were more complex.

In order to properly describe thermal effects on the DSC curves, let us to introduce a schematic phase diagram that shows the phase relationships between four phases (water, ice, L_β, and L_α) (Fig. 4). This phase diagram was constructed using the phase rule and other rules for construction of phase diagrams [25] and taking into account that liquid water and the L_α phase are high-temperature phases in relation to the ice and the L_β phases, respectively. With the aid of the phase diagram, the DSC heating curves of samples with water contents ≥11 wt% (curves a–f, Fig. 3) are described as follows. In fully hydrated samples and in samples equilibrated at RH = 100% through the vapor phase (over pure water), two endothermic peaks, T_{m1}^{i} and T_{w}^{i}, were observed around 0°C (Fig. 3, curves a and b) and are assigned to the L_β+ice→L_α+ice and L_α+ice→L_α+water invariant phase transitions, respectively. The heating pathway is shown in Fig. 4 as the 11′ line. Superscripts i and m refer to the invariant and monovariant phase transitions, respectively, whereas subscripts w and m refer to the ice melting and the lipid chain melting transition ('main transition'), respectively. For samples that were dehydrated at 2.5 MPa (17–19 wt% water, Fig. 3, curve c) a major endothermic peak, T_{m1}^{i}, with a high-temperature shoulder, T_{w1}^{m} preceded the T_{bh}. The T_{w1}^{m} thermotropic event was assigned to the L_α+ice→L_α phase transition; the heating path-

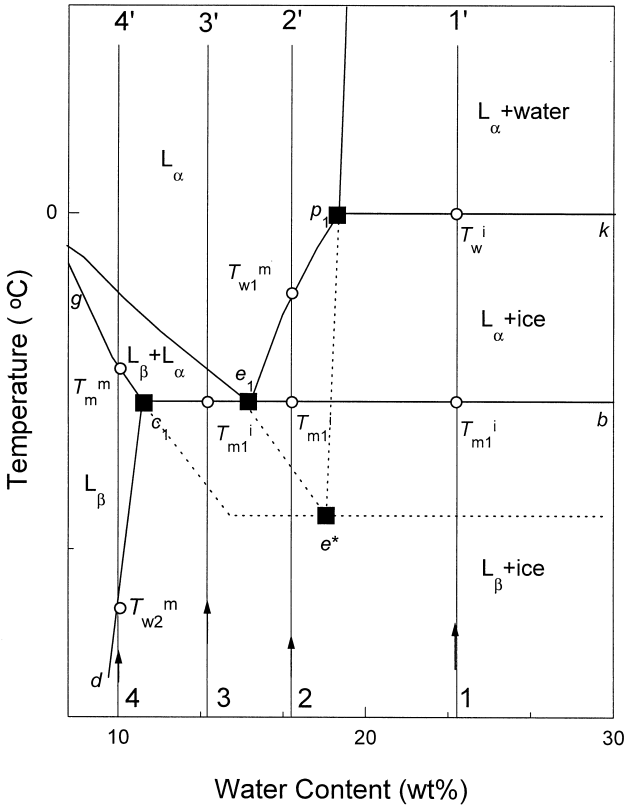

Fig. 4. Schematic phase diagram that illustrates phase transition sequence during heating of DOPE with water content more than 10 wt%. Circles represent correspondence between thermotropic events on DSC heating curves and the equilibrium phase transition temperatures. Squares represent specific points of the phase diagram, namely, eutectic e_1, metastable eutectic, e^*, peritecitc p_1, and point c_1 which corresponds to the maximal solubility of water in the L_β phase in the equilibrium with the ice phase. Vertical lines 11′, 22′, 33′, 44′ represent heating pathways for DOPE samples with different water content. Dotted lines represent metastable equilibrium.

way is shown as line 22′ in Fig. 4. An endothermic peak around 0°C (marked with an asterisk in Fig. 3), which was also observed in the samples with water contents of 17–19 wt%, is most likely an artifact due to the melting of ice that condensed on the lid of the DSC pan [26,27]. Indeed it has been observed that the magnitude of this effect increased in consecutive DSC scans as expected (DSC curves not shown). In samples that were dehydrated at 4 and 8 MPa (water content 13–16 wt%, Fig. 3, curves d and e), the major endothermic peak, T_m^i, is associated with the L_β+ice$\rightarrow L_\beta+L_\alpha \rightarrow L_\alpha$ phase transition; the heating pathway is shown in Fig. 4 as line 33′. The two endothermic peaks that were observed in DSC curves of samples dehydrated at 15 MPa (water content about 11 wt%, Fig. 3, curve f) were assigned to the L_β+ice$\rightarrow L_\beta$, T_{w2}^m, and $L_\beta \rightarrow L_\alpha+L_\beta \rightarrow L_\alpha$, T_m^m monovariant phase transitions; the heating pathway is shown as line 44′ in Fig. 4.

DSC curves for samples dehydrated at 35 and 57 MPa have a completely different appearance. A weak endothermic peak slightly below 0°C, T_{m2}^i, and a strong endothermic peak centered at 25°C, T_c, were observed during the first heating DSC scans (Fig. 3, curves g and h). On the second and successive scans, the high-temperature endothermic peak disappeared as shown in Fig. 5. DSC curves obtained during the second heating scans had an exothermic peak followed by the endothermic peak. However, when the scanned samples were kept at 0°C for 2 days, the T_c peak was again present in the first DSC heating curve, which was similar to the original samples (curves not shown). Such apparent irreversibility in the thermal behavior of the phospholipid:water mixtures is usually associated with the lamellar crystalline phase, L_c [5]. The X-ray diffraction data confirmed the appearance of the L_c phase, and allowed us to identify the thermotropic events on the DSC heating curves as follows. The minor endotherm, T_{m2}^i, which was observed slightly below 0°C, is assigned to the $L_c+L_\beta \rightarrow L_c+H_{II}$ phase transition. From the X-ray diffraction data, the patterns of the L_c phase did not change in the T_{m2}^i temperature range, whereas the *d*-spacing for the minor reflection decreased sharply. The major endotherm, T_c, with an onset temperature of about 20°C is assigned to the $L_c+H_{II} \rightarrow H_{II}$ phase transition because lamellar small-angle reflections and the sharp wide-angle reflections disappeared on the X-ray diffraction patterns between 15 and 25°C.

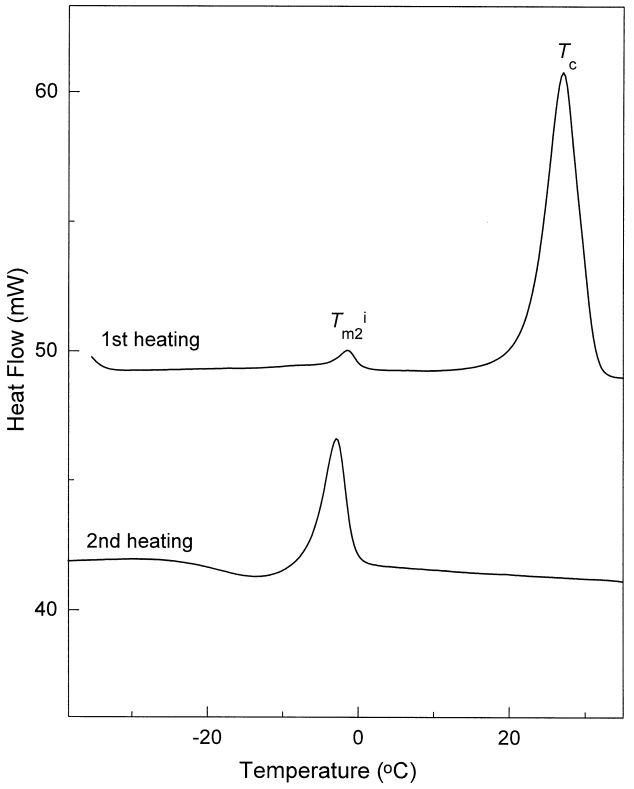

Fig. 5. Representative subsequent DSC heating curves of DOPE liposomes dehydrated at 0°C at 34.5 MPa showing apparent irreversibility of the $L_c \rightarrow H_{II}$ phase transition (T_c peak). Heating rate: 40°C/min.

For samples that were dehydrated at 137 and 276 MPa, the T_c peak was no longer observed. Instead, one or two weak and broad endothermic peak(s) appeared between −50 and −20°C (Fig. 3, curves i and j and inset). These thermal events were not accompanied by major structural changes because the X-ray diffraction patterns were the same in the temperature range from −45 to 50°C. The nature of these thermal events is unclear.

DOPE that was hydrated from the dried state at 0°C exhibited similar thermal behavior as DOPE liposomes dehydrated at 0°C (curves not shown). Changes in the general appearance of the DSC curves were observed in the same osmotic pressure ranges: the T_c peak appeared in the DSC heating curves after equilibration at 57 MPa and 35 MPa, and disappeared after equilibration at ≤15 and ≥137 MPa.

Summarizing data obtained for DOPE after equilibration at 0°C, it can be concluded that the $P_\delta \leftrightarrow L_c$ and $L_c \leftrightarrow L_\alpha$ lyotropic phase transitions occurred when DOPE was equilibrated at 0°C between 137 and 57 MPa, and 35 and 15 MPa, respectively. These lyotropic phase transitions are fully reversible; and they were observed in the same osmotic pressure interval when DOPE was both dehydrated from the fully hydrated state and hydrated from the dried state. This observation is in agreement with the results of Pohle and Selle [16]; they did not observe hysteresis between hydration and dehydration when equilibration was performed at 28°C.

3.2.3. Partially hydrated DOPE: 29°C equilibration

Representative DSC heating curves for DOPE dehydrated in the H_{II} phase at 29°C are shown in Fig. 6. DSC curves for samples dehydrated at 0–16 MPa (water content from 23 to 10 wt%, Fig. 6, curves a–d) and 158 and 305 MPa (water content <1 wt%, curves h and i) are similar to those of samples equilibrated at 0°C with a similar water content. The description of the DSC curves for samples with water contents $\geq$10 wt% is given above (DSC results, 0°C equilibration), and will not be repeated here. At water contents less than about 8 wt% (osmotic pressure $\geq$25 MPa, Fig. 6, curves e–i), DSC curves obtained after cooling to both −15°C (not shown) and −140°C were identical indicative that ice formation did not occur in these samples. Note that this is the same water content range (9–11 wt% water) below which ice formation was not observed during the X-ray diffraction experiments. DOPE samples that were dehydrated at 25 MPa (water content about 8 wt%, curve e) exhibited a major endotherm (assigned to the invariant $L_\beta+H_{II} \rightarrow L_\alpha+H_{II}$ or $L_\beta+L_\alpha \rightarrow L_\alpha+H_{II}$ phase transition) and a weak T_{bh} peak. For samples dehydrated at 40 MPa (water content about 5 wt%, curve f), a single endothermic peak was observed; the $L_\alpha \rightarrow H_{II}$ phase transition disappeared. Note also that in those samples a weak endothermic step at about −40°C, which had an appearance of the glass transition, was observed; this effect is currently under investigation. An exothermic peak between −40 and −20°C followed by an endothermic peak were observed in the DSC curves for samples dehydrated at 81 MPa (water content about 3 wt%, curve g, and inset). The endothermic peak for these samples is assigned to the $L_\beta \rightarrow H_{II}+L_\beta \rightarrow H_{II}$ phase transition sequence.

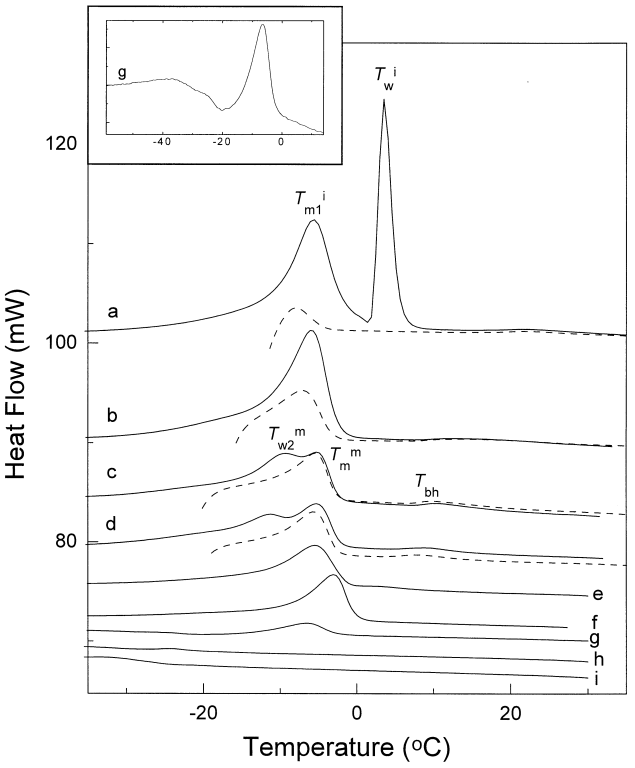

Fig. 6. Representative DSC heating curves of DOPE liposomes dehydrated at 29°C through vapor phase equilibration. Heating rate: 40°C/min. Broken curves: DSC runs that were performed from −15 to −20°C. Solid curves: scans were performed from −140°C. (a) Equilibrated at 0 MPa, 23.7 wt% water; (b) 4 MPa, 13.6 wt% water; (c) 11 MPa, 11.0 wt% water; (d) 16 MPa, 10.0 wt% water; (e) 25 MPa, 7.7 wt% water; (f) 40 MPa, 5.9 wt% water; (g) 81 MPa; (h) 158 MPa, 0.5 wt% water; (i) 305 MPa, 0.0 wt% water. Inset: DSC heating curve of DOPE dehydrated at 81 MPa.

DSC heating curves for DOPE hydrated from the dried state at 29°C are very similar to those that were obtained after dehydration of DOPE from the fully hydrated state (the curves not shown); hysteresis between sorption and desorption was not observed.

Phase transition temperatures as a function of water content are given in the Appendix.

3.3. Water sorption isotherms

Sorption/desorption isotherms for DOPE at 0°C and 29°C are given in Fig. 7. The water content of

samples dehydrated from the fully hydrated state was slightly higher than in samples hydrated from dried state; however, in most cases the difference was within experimental uncertainty. At 29°C, the water content of the H_{II} phase gradually decreased with osmotic pressure; the dependence between water content and logP is approximately linear (Fig. 7, top). At 0°C (Fig. 7, bottom), the water content of the L_α phase decreased approximately linearly with logP up to about 11 wt% at 15 MPa; at 35 MPa, water content decreased sharply to about 2.5 wt%.

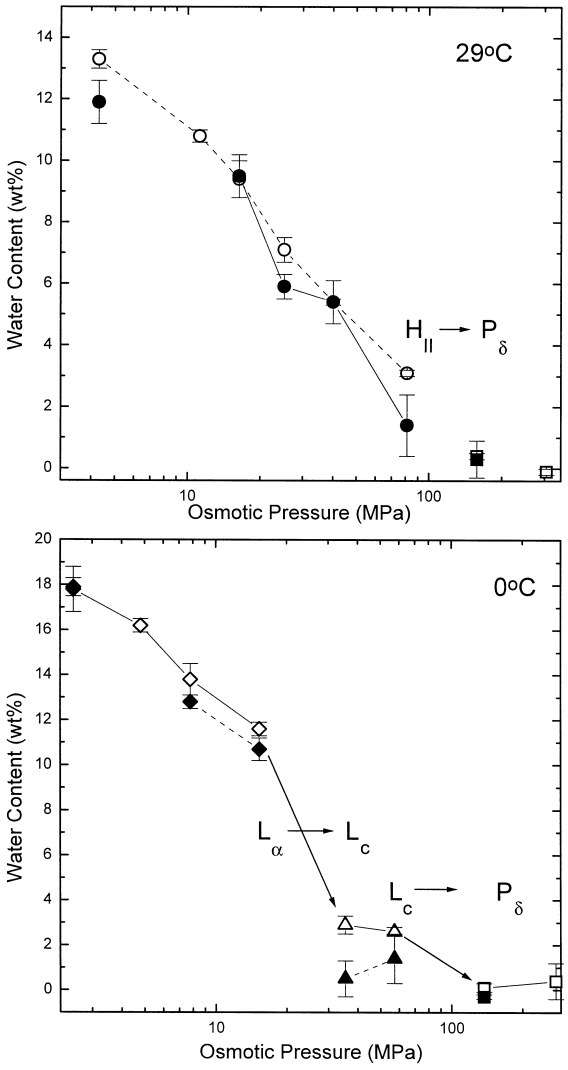

Fig. 7. Desorption/sorption isotherms of DOPE at 29°C (top) and at 0°C (bottom). Open symbols: desorption; closed symbols: sorption. □, ■: P_δ phase; ◇, ◆: L_α phase; ○, ●: H_{II} phase; △, ▲: L_c phase.

This discontinuity in the sorption isotherm is associated with the lyotropic $L_\alpha \rightarrow L_c$ phase transition. According to the dehydration experiments, the water content of the L_c phase is about 2.5–3.0 wt% at both 35 and 57 MPa and corresponds to the monohydrate DOPE·H_2O. The fact that hydration of the L_c phase was similar at two different osmotic pressure indicates that this is a stoichiometric monohydrate. At osmotic pressures of 137 and 276 MPa, the water content decreased to 0 wt% when the L_c phase transformed into the P_δ phase.

Hydration of the L_α and H_{II} phases of DOPE has been reported in the literature [8,11]. Hydration of the H_{II} phase determined by Gawrisch et al. [11] at 22°C is higher than that obtained by Webb et al. [8] at 20°C. The results obtained in this study are intermediate between those two sets of data. Agreement between this study and [11] for the H_{II} phase at osmotic pressures of 20–30 MPa is satisfactory; however at osmotic pressures <10 MPa, hydration of DOPE in both the H_{II} and L_α phase from [11] is higher than that obtained in this study. The possible reason for this difference is due to a difference in the preparation procedure: the samples in [11] were hydrated with the aqueous solutions of polymer whereas in this study DOPE was hydrated through vapor phase equilibration.

4. Discussion

The part of the phase diagram reported in [11,15] describes equilibria involving three phases (H_{II}, L_α, and bulk water phase) at water contents ≥ 5 wt% and temperatures above 0°C. In this work, the L_β, L_c, and P_δ phases, and the ice phase were also observed. According to the water sorption data, the L_c phase is likely to be a stoichiometric crystallohydrate DOPE·H_2O. The phase diagram which includes five lipid phases and two water phases is shown in Fig. 8. The phase diagram was constructed using DSC and X-ray diffraction data from this work together with the literature data on the L_α/H_{II}/water phase equilibria [11,15]. Construction of the phase diagram is described in the supplementary materials in detail. Uncertainty in determination of the coordinates of the specific points on the phase diagram is estimated to be within 3–5°C and 2–3 wt% of water. There is a

gap at 7–10 wt% water below 0°C; the lack of experimental data did not allow us to construct this part of the phase diagram. There is also an uncertainty about the low-water content part of the phase diagram; the minor phase that coexists with the L_c phase in the low-water content part of the phase diagram was provisionally identified from the X-ray diffraction experiments as the L_β phase below 0°C and H_{II} phase above 0°C, and the corresponding part of the phase diagram was constructed based on this assumption. Lack of higher-order diffractions did not allow for certainty about identification of those phases.

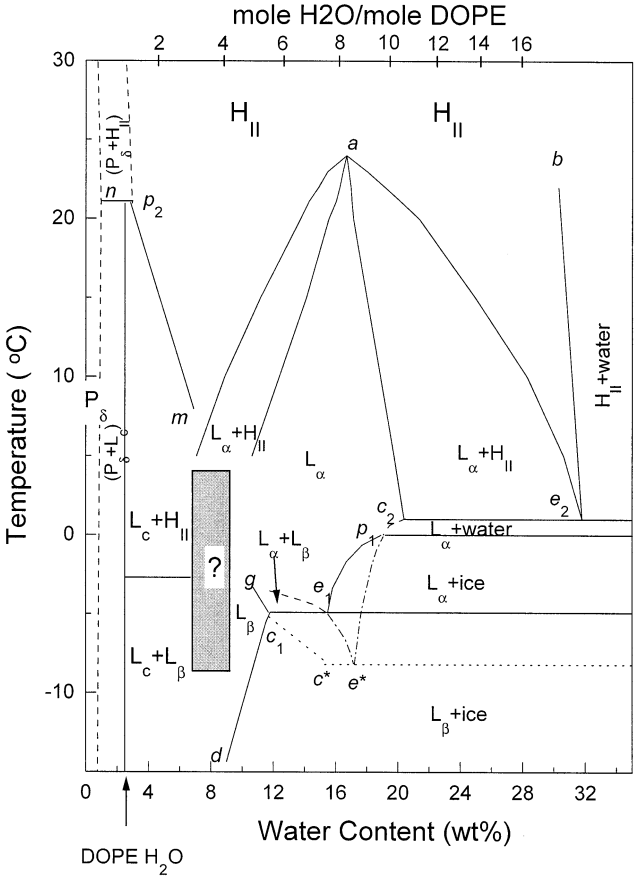

Fig. 8. Phase diagram of the DOPE:water system. Solid and dash lines represent equilibrium phase borders whereas dot and dot-and-dash lines represent metastable phase equilibrium. Phase borders which are shown by dash and dot-and-dash lines were drawn approximately; no experimental data points were used to construct those lines. Phases which are shown in brackets were not observed in the X-ray diffraction experiments. Part of the phase diagram which is shown in the rectangle with a question mark has not been constructed due to lack of experimental data.

Detailed phase diagrams have been reported for several synthetic saturated PE:water systems by Seddon et al. [3] and Caffrey [28], and for an unsaturated species of PE, POPE, by Marinov and Duforc [29]. Phase diagrams for all of these systems have some common features with each other and with the phase diagram of the DOPE:water system constructed in this study (Fig. 8), which are as follows. The gel-to-liquid crystal phase transition temperature, T_m, of DOPE increased with dehydration as expected [30]; however, the increase in T_m was relatively small, only a few °C (line c*g, Fig. 8). A similar small increase in the T_m with dehydration was observed for POPE [29] and saturated species of PE [3,28] where the difference in T_m between the fully hydrated and the dehydrated lipid did not exceed 10°C.

The L_c phase was observed in fully hydrated saturated species of PE that were annealed for several hours [3,31]. However, the L_c phase was not detected in the fully hydrated state of a saturated species of PE with longer chains, DAPE. In DAPE, the L_c phase formed only after extensive dehydration, at water contents <3 wt%. Similar behavior of the L_c phase was observed for DOPE in the present study. The L_c phase did not form at water contents >11 wt% even after annealing for 2 weeks at 0°C, but formed after dehydration at water contents <7 wt% when the samples were annealed for at least 2 days at 0°C. Similar to the L_c phase of DPPC and several saturated species of PE [3,31–34], the L_c phase of DOPE is characterized by slow kinetics of formation. In DDPE and DAPE at low water contents, the L_c phase transformed into the H_{II} phase upon heating; the same $L_c \rightarrow H_{II}$ thermotropic phase transition was observed in DOPE. The thermotropic phase transitions of the L_c phase of DOPE observed in this work are presented in Scheme 1.

$$L_c\,(-40...15°C) \rightarrow H_{II}\,(25°C) \rightarrow L_\beta\,(-15°C) \rightarrow L_c\,(0°C, 2\ days)$$

Scheme 1.

It should be mentioned that the L_c phase in DOPE had different hydration properties compared with the L_c phase of saturated species of PE. DOPE in the L_c phase contains water of hydration, whereas saturated species of PE in the L_c phase are anhydrous [3]. When the water of hydration was removed from DOPE, the L_c phase transformed in the P_δ phase

whereas in saturated PE species [3] the L_c phase persisted to close to 0 wt% water content. Note that one of the PE species with one mono-unsaturated chain, POPE, did not form a crystallohydrate; the L_c phase in POPE was observed even at 0 wt% water content [35], which is similar to the behavior of saturated species of PE.

There is a difference in the L_α/H_{II} phase relationships between DOPE and other synthetic phospholipids studied to date. The T_{bh} of DOPE first increased with dehydration ([11] and Fig. 8) and then decreased, whereas in saturated species of PE [3,29], the T_{bh} decreased with dehydration. This unusual phase behavior has been discussed in detail previously [11,15,36], and is not discussed in this work.

A special feature of the DOPE:water system is that the gel-to-liquid crystal phase transition occurred below 0°C (below water freezing point). To the best of the authors' knowledge, phase diagrams for a phospholipid:water system that describe both phospholipid phase transitions and ice/water phase equilibria have not been reported in the literature, despite numerous studies of ice formation and melting [26,37–40]. The low-temperature part of the phase diagram of the DOPE:water system constructed in this study describes both the lipid phase transition and the ice melting, which allowed us to describe the freeze-induced dehydration of DOPE in quantitative manner. Freeze-induced dehydration of membrane lipids is the primary mechanism responsible for the freeze-induced destabilization of biological membranes [2]. One way to obtain a quantitative estimate of the extent of freeze-induced dehydration under near-equilibrium conditions (when the water diffusion is not a limiting step) is to compare the hydration of the lipid in equilibrium with the ice phase, and the hydration of the lipid phase in metastable equilibrium with liquid water at the same temperature as described below.

On the phase diagram (Fig. 8), line $c_2p_1e^*$ describes the hydration of DOPE in the L_α phase in equilibrium with liquid water, line p_1e_1 corresponds to the hydration of DOPE in the L_α phase in equilibrium with the ice phase, and line c_1d describes hydration of the L_β phase in equilibrium with the ice phase. Dotted and dot-and-dash lines in Fig. 8 represent metastable equilibrium. There are several possible freezing pathways that differ in the temper-

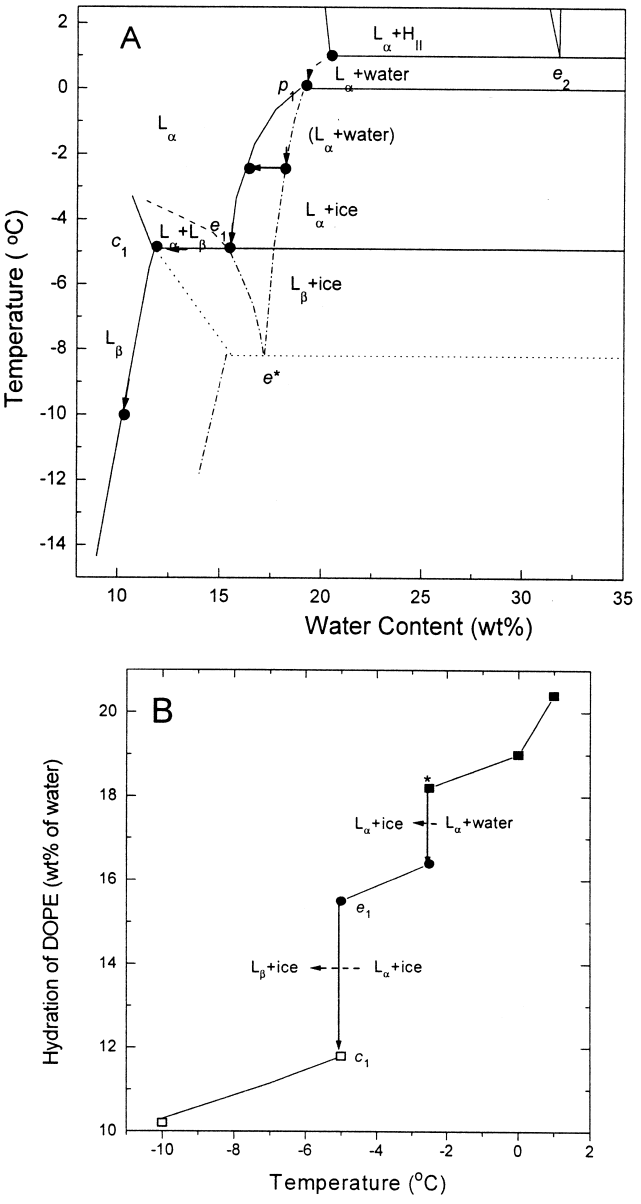

Fig. 9. Change of DOPE hydration during cooling when water crystallization occurs between peritectic and equilibrium eutectic temperatures. (A) Part of the phase diagram of DOPE:water system. Arrows show change of hydration of DOPE during cooling; circles show points at which hydration of DOPE was calculated. Hydration of DOPE is shown as a function of the temperature in B. (B) Hydration of DOPE as a function of temperature. ■: hydration of the L_α phase in equilibrium with liquid water; ●: hydration of the L_α phase in equilibrium with ice; □: hydration of the L_β phase in equilibrium with ice. Solid arrows show direction of changes in DOPE hydration during cooling; dash-arrows indicate phase transitions. Symbols marked with an asterisk show metastable equilibrium.

ature at which ice nucleation occurs. Temperature of the ice nucleation depends on a number of factors such as cooling rate and number and nature of heterogeneous nucleation centers, and the ice nucleation is a random event and can occur in relatively wide temperature range below 0°C. One of the possible freezing pathways is shown in Fig. 9 together with the temperature dependence of the DOPE hydration as determined from the phase diagram. Fig. 9 describes a case when ice formation occurs at −2.5°C, in the field where L_α+ice is the equilibrium state. The change of lipid hydration with temperature was determined from the phase diagram and is shown in Fig. 9B. The water content decreases from 20 wt% to 18 wt% over the temperature range of 1 to −2.5°C, which is followed by a reduction in hydration from 18 wt% to 16 wt% as a result of the ice formation at −2.5°C. With further cooling, the water content decreases from about 16 wt% to 12 wt% due to the $L_\alpha \rightarrow L_\beta$ lipid phase transition.

The considered example shows that freeze-induced dehydration of DOPE is not dramatic, only a few wt%. It should be stressed that any direct comparisons of DOPE phase behavior with freeze-induced dehydration and freeze-induced membrane phase transitions in more complex systems, such as plant membranes, should be made with caution. The freeze-induced phase transition sequence in biological membranes is likely to be more complex than in DOPE. Indeed, the hydration of DOPE (and other PE species) is significantly less than other phospholipid species such as PC, which have higher hydration in equilibrium with water [8]. The effect of freezing on lipid hydration in such lipids can be more substantial, i.e. a greater amount of water could be removed during freezing. There is also the expected difference in the phase transition sequence during freezing. Plant membranes contain a number of different phospholipid species, and one of the possible consequences of freezing would be lipid-lipid demixing. Studies of dehydration-induced lipid-lipid demixing above 0°C have been reported in earlier papers from this laboratory [8–10]. We believe that construction of the low-temperature parts of the corresponding phase diagram is a useful approach for quantitative studies of freeze-induced phase transitions in model phospholipid mixtures and biological membranes.

Acknowledgements

This work was supported by Grant DE-FG02-84ER13214 from the United States Department of Energy. We wish to thank Dr. Ernest Fontes for his expert assistance in carrying out the X-ray diffraction experiments.

Appendix. Supplementary materials

Construction of the phase diagram of DOPE:water system

Step-by-step description of the procedure used to construct the phase diagram is provided below; such a detailed description may be useful to those readers who do not have a strong material science background. In order to construct the phase diagram, it is necessary to draw phase borders that divide the areas belonging to the different phases. In a two-component system at a constant pressure, those borders are represented by lines and describe either invariant equilibria when three phases coexist (e.g. L_β+ice/L_α+ice) or monovariant equilibria when two phases coexist (e.g. L_β+ice/L_β). Invariant equilibria are represented by straight lines that are parallel to the composition axis whereas monovariant equilibria are represented by lines that are neither horizontal nor vertical.

To use DSC data for construction of a phase diagram, it is necessary to assign a characteristic point on the DSC peak to a phase transition temperature. This is not as straightforward as it might appear. There are five characteristic points on DSC peaks (the onset, the extrapolated onset, the peak, the extrapolated completion, and the completion) [S1], and any of these points may be chosen to represent a phase transition temperature. In phospholipid studies, the extrapolated onset and extrapolated completion temperatures [S2,S3] and the peak temperature [S4] have been widely used. In the present study, the extrapolated onset temperature was chosen to represent the $L_\alpha \rightarrow L_\alpha + H_{II}$ phase transition (T_{bh} peak), the $L_c + H_{II} \rightarrow H_{II}$ phase transition (T_c peak), and the invariant L_α+ice/L_α+water phase transition (T_w^i thermotropic event) as shown in Fig. S1. Peak temperature was chosen to represent the invariant phase

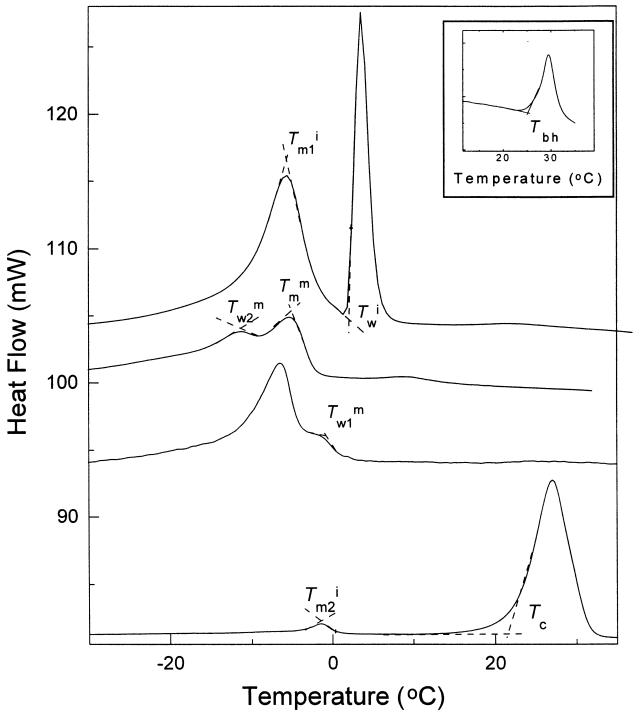

Fig. S1. Determination of the phase transition temperatures from DSC curves. The thermotropic events on DSC heating curves correspond to the following phase transitions: T_{m1}^{i}: L_β+ice→L_α+ice; T_{w}^{i}: L_α+ice→L_α+water; T_{w2}^{m}: L_β+ice→L_β; T_{m}^{m}: L_β→L_β+L_α; T_{w1}^{m}: L_α+ice→L_α; T_c: L_c+H_{II}→H_{II}; T_{m2}^{i}: L_c+L_β→L_c+H_{II}. Inset: T_{bh}: L_α→L_α+H_{II}.;

transitions L_β+ice→L_α+ice (T_{m1}^{i} thermotropic event) and L_c+L_β→L_c+H_{II} (T_{m2}^{i} thermotropic event) and monovariant phase transitions L_α+ice→L_α (T_{w1}^{m} thermotropic event), L_β+ice→L_β (T_{w2}^{m} thermotropic event), and L_β→L_β+L_α (T_{m}^{m} thermotropic event). It should be noted that for invariant phase transitions, the onset temperature would be a more correct choice. However, it was difficult to establish the baseline and determine the onset temperature for those thermal events, and the peak temperature was chosen because it gave more reproducible results. Note that such a compromise is not unusual in DSC studies of phospholipid:water systems [S5].

Three parts of the phase diagram for the DOPE:water system were constructed separately, and then combined in a single phase diagram. Let us first consider construction of the low-temperature part. The part of the phase diagram of the DOPE:water system in the low-temperature range is shown schematically in Fig. 4 of the paper itself. This phase diagram consists of three characteristic points: eutectic point e_1, peritectic point p_1, and point c_1, which corresponds to the maximal solubility of water in the L_β phase. Fig. S2 shows the experimentally determined phase transition temperatures in the low-temperature region. Experimental points that correspond to the invariant eutectic (L_β+ice→L_α+ice) and peritectic (L_α+ice→L_α+water) phase transitions are shown as squares and up triangles, respectively, and points that correspond to the monovariant L_β+ice→L_β and L_α+ice→L_α phase transitions are shown as

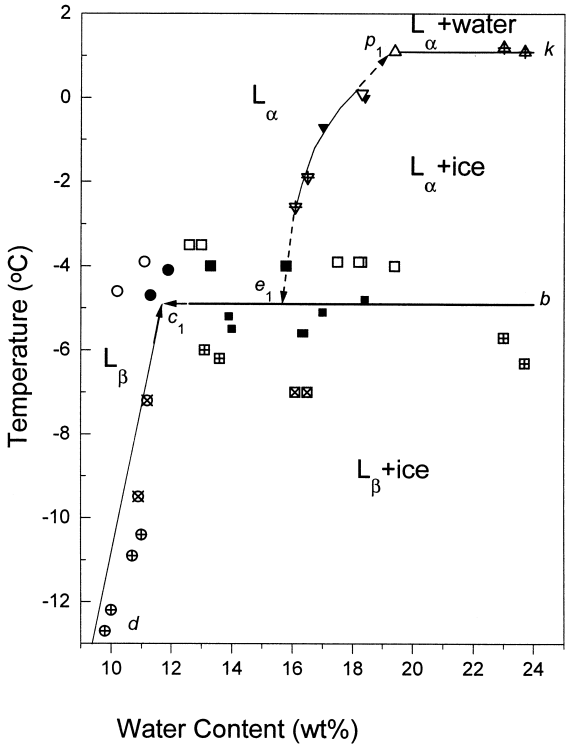

Fig. S2. Part of the DOPE:water phase diagram at >10 wt% water near and below 0°C constructed from the DSC data. Squares: T_{m1}^{i} thermotropic event on the DSC heating curves due to invariant eutectic melting L_β+ice→L_α+ice or L_β+ice→L_β+L_α; circles: T_{w2}^{m} thermotropic event on DSC heating curves due to the L_β+ice→L_β monovariant phase transition; down triangles: T_{w1}^{m} thermotropic event on DSC curves due to the L_α+ice→L_α monovariant phase transition; up triangles: T_{w}^{i} thermotropic event on DSC heating curves due to the L_α+ice→L_α+water invariant peritectic phase transition. Different types of symbols belong to DOPE samples prepared in different ways: □, ○, △, ▽: hydration at 0°C; ■, ●, ▲, ▼: dehydration at 0°C (smaller and larger symbols represent two independent preparations); ⊠, ⊗: hydration at 29°C; ⊞, ⊕, plus in up triangle, plus in down triangle: dehydration at 29°C. Broken lines and arrows show extrapolation procedure.

circles and down triangles, respectively. Different types of symbols (closed, open, 'x'-centered and '+'-centered) were used to represent results obtained for DOPE samples that were prepared in different ways (obtained by hydration and dehydration at 29 and 0°C) as described in the legend for Fig. S2. Note that the L_β+ice$\rightarrow L_\alpha$+ice and L_β+ice$\rightarrow L_\beta$ phase transition temperatures for samples equilibrated at 0°C are higher than those for samples equilibrated at 29°C. The reason for this difference is unclear; however, the trend in the change of the phase transition temperatures with water content is the same and independent of the manner of preparation. The L_β+ice$\rightarrow L_\alpha$+ice phase transition temperature is approximately constant at water contents between 12.5 and 23 wt%. At water contents of 10–12 wt%, the L_β+ice$\rightarrow L_\beta$ phase transition temperature decreases with decreasing water content. The data for different types of preparations were treated together. Temperatures of the eutectic phase transition (squares in Fig. S2) were averaged for different types of preparations, and the average temperature (-4.9 ± 1.6°C) was taken as the eutectic temperature. To determine the composition corresponding to the eutectic point, curve e_1p_1 (down triangles) was graphically extrapolated to the eutectic temperature −4.9°C, and composition of the point e_1 was determined from the graph as shown by the arrow in Fig. S2; the eutectic composition is equal to 15.5 wt% water. The peritectic temperature for the phase transition L_α+ice$\rightarrow L_\alpha$+water (up triangles) is equal to 1.0 ± 0.5°C as determined from the DSC heating curves. The composition corresponding to the peritectic point was determined by graphical extrapolation of curve e_1p_1 to 1°C; the peritectic composition is equal to 19.2 wt% water. Note that the temperature of the peritectic phase transition L_α+ice$\rightarrow L_\alpha$+water has to be equal to the melting temperature of pure ice. Hence, 0°C was chosen to represent the temperature of the peritectic reaction on the phase diagram. To determine the coordinates of point c_1, the data for the L_β+ice$\rightarrow L_\beta$ phase transition for four preparations (circles in Fig. S2) were described by linear regression equation (line c_1d), and the intersection of this line with the eutectic line at −4.9°C gave a composition of 11.8 wt% water. It is also possible to estimate the position of the gc_1 line (Fig. 4 of the paper), which describes $L_\beta\rightarrow L_\alpha$+$L_\beta$ phase transition; this phase transition corresponds to the thermotropic event T_m^m on the DSC heating curves. The T_m^m data were not included in Fig. S2 for clarity. Four DOPE samples that were equilibrated at 0°C (water content 10.2–11.9 wt%) gave an average T_m^m of -1.4 ± 0.2°C, and four samples that were equilibrated at 29°C (water content 9.8–11.9 wt%) gave an average T_m^m of -5.2 ± 0.2°C. The narrow water content region and scatter of the experimental points did not allow us to accurately construct the T_m^m vs. water content curve (gc_1 line); however, we estimated the approximate position of this line by connecting point c_1 with the point that was taken as the average of eight samples (average $T_m^m=-3.3\pm2.0$°C and average composition at 10.7 wt% water). The gc_1 line is not shown in Fig. S2 for the sake of clarity.

DSC data for the $L_\beta\rightarrow L_\alpha$ phase transition temperature (T_m) that were obtained for supercooled sam-

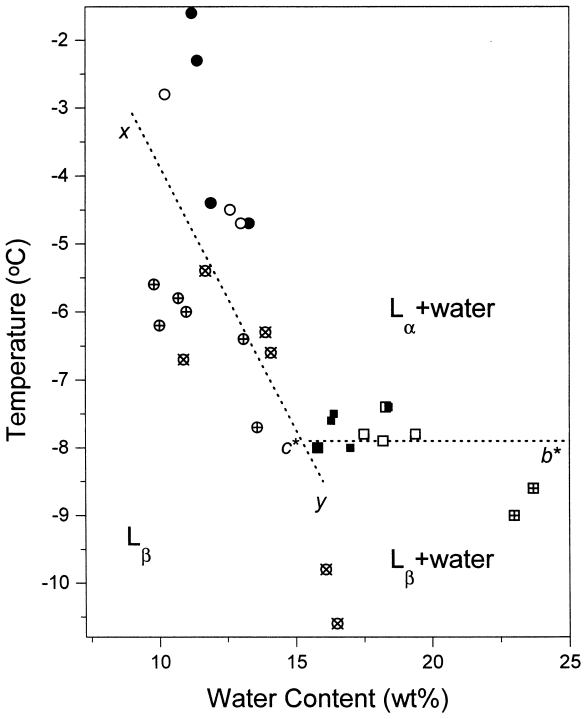

Fig. S3. DSC data for DOPE with >10 wt% water that were obtained for supercooled samples in the absence of ice. Squares: metastable phase equilibrium L_β+water$\rightarrow L_\alpha$+water; circles: metastable phase equilibrium $L_\beta\rightarrow L_\alpha$+$L_\beta$. See Fig. S2 for explanation of symbols representing different ways of preparation of partially hydrated DOPE samples. Point c^* corresponds to maximal solubility of water in the L_β phase in the presence of liquid water.

ples (in the absence of ice) are shown in Fig. S3. T_m was approximately constant and equal to -7.9 ± 0.5°C up to a water content of approximately 15 wt%; above this water content, the T_m increased with decreasing water content. The water content above which T_m starts to increase has been determined graphically as the intersection point of horizontal line c^*b^* ($T = -7.9$°C) and line xy; line xy represents the fit of the experimental points (circles in Fig. S3) to a linear regression equation. The water content estimated from this procedure is equal to 15.3 wt%. This point, c^*, corresponds to the maximal solubility of water in the L_β phase that is in metastable equilibrium with liquid water. It is also possible to estimate the coordinates of the metastable eutectic L_β+water → L_α+water. This point, e^*, is the intersection point of the continuation of the lines that describe the $L_\beta+L_\alpha \rightarrow L_\alpha$ and L_α+water → L_α monovariant phase transitions into the metastable region (see Fig. 4, dotted lines). Hence the composition of this metastable eutectic point is located somewhere between 15.5 wt% water (equilibrium eutectic composition, e_1) and 19.2 wt% (peritectic composition, p_1). We take the average between these two values (17.4 wt%) as an estimate of the composition of metastable eutectic.

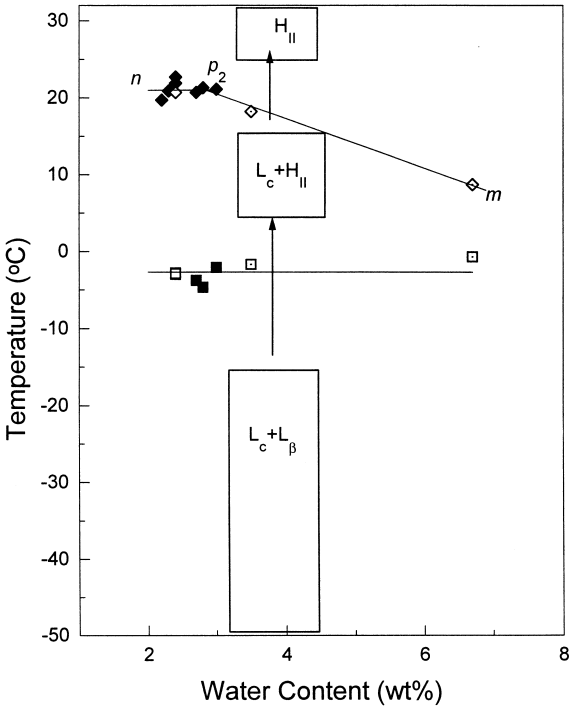

Fig. S4. Part of the DOPE:water phase diagram at 2–7 wt% water constructed from the DSC and X-ray diffraction data. □, ■, dot in square: T^i_{m2} thermotropic event on DSC heating curves due to the $L_c+L_\beta \rightarrow L_c+H_{II}$ invariant phase transition; ◇, ◆, dot in diamond: T_c thermotropic event on DSC curves due to the $L_c+H_{II} \rightarrow H_{II}$ or $L_c+H_{II} \rightarrow P_\delta+H_{II}$ phase transitions. Open symbols represent results obtained for hydrated samples, closed symbols are for dehydrated samples, and dot-centered symbols are for DOPE samples which were dehydrated at 29°C followed by annealing in sealed DSC pans at 0°C for several days. Boxes represent composition/temperature regions of existence of corresponding phases as obtained from the X-ray diffraction experiments.

The DSC data for samples with water contents of 2–7 wt% that were equilibrated at 0°C are shown in Fig. S4 together with the X-ray diffraction data. According to the X-ray diffraction data (Fig. S4, boxes), these samples undergo the phase transition sequence $L_c+L_\beta \rightarrow L_c+H_{II} \rightarrow H_{II}$ during heating. The $L_c+L_\beta \rightarrow L_c+H_{II}$ phase transition is an invariant phase transition according to the phase rule because three phases participate. The DSC data show that the phase transition temperature is approximately constant at water contents from 2 to 7 wt% and equal to -2.7 ± 1.3°C. In samples with water contents of 2–3 wt% the $L_c \rightarrow H_{II}$ phase transition temperature (T_c peak) is 21.1 ± 0.9°C and decreased to about 7°C when the water content increased from 3 to 7 wt%.

Part of the phase diagram at water contents >5 wt% and temperatures above 0°C has been constructed in [S6,S7]. Note that the temperature of the phase transition L_α+water/H_{II}+water is assumed to be 1°C in [S6], and 10°C in [S7]. In this paper, we take 1°C for the temperature of this invariant phase transition. It should be noted that there is a quantitative difference between the X-ray diffraction and DSC data obtained in this study for the $L_\alpha/L_\alpha+H_{II}$ phase equilibria; DSC gave higher transition temperatures than X-ray diffraction. Most likely, the difference is due to the slow kinetics of the $L_\alpha \rightarrow H_{II}$ phase transition. In such cases, DSC gives a higher apparent phase transition temperature than the equilibrium value. According to [S8], the $L_\alpha \rightarrow H_{II}$ phase transition in fully hydrated DOPE is very slow in the vicinity of the phase transition temperature, and higher values for the phase transition temperatures may reflect the fact that insufficient time was used to determine the phase transition temperature. This is the reason why we did not use DSC data to describe

the L_α/H_{II} phase equilibrium. Fig. S5 shows the X-ray diffraction data that are reported in [S6] (Fig. 5 in [S6]) together with the data from this study. Drawing the phase borders that are represented by lines *sa*, *au*, ac_2, ae_2 does not require comment. Line e_2b (H_{II}+water/H_{II} phase equilibrium) was constructed by connecting eutectic point e_2 and one point that was reported in [S6] for the limited hydration of the H_{II} phase (30.3 wt% water at 22°C).

The three parts are combined together in Fig. 8 of the paper. To construct the low-water content part of the phase diagram, we assumed that DOPE·H_2O crystallohydrate melts incongruently, i.e. the composition of the liquid produced by melting is different from the composition of crystallohydrate (see [S9] for a description of phase diagrams with crystallohydrates). The water content corresponding to the peritectic point p_2 was determined as the intersection of lines np_2 and p_2m in Fig. S5 and equal to 2.8 wt% of water. The field of existence of the P_δ phase is shown at a water content <1 wt%, according to the X-ray diffraction data. Fields P_δ+L_c and P_δ+H_{II} (shown in brackets) were added to be consistent with the rules of the construction of phase diagrams; however, we do not have X-ray diffraction data in this range of water contents. There is a gap at 7–10 wt% water below 0°C. In this region, only three DSC samples with water contents of 7.7, 9.0, and 9.1 wt% were analyzed; the lack of experimental data does not allow for construction of this part of the phase diagram.

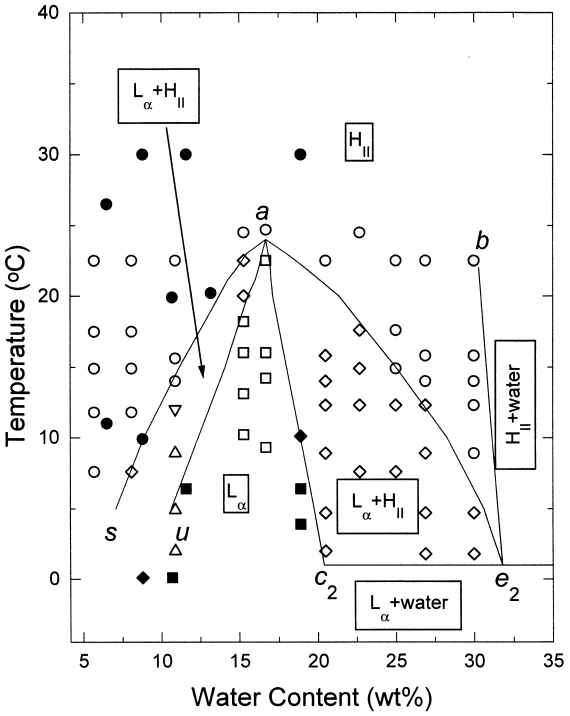

Fig. S5. Part of the phase diagram of the DOPE:water system at water content >5 wt% above 0°C from the X-ray diffraction data. This work: close symbols; [S6]: open symbols. ●, ○: H_{II} phase; ◆, ◇: L_α+H_{II}; ■, □: L_α; △: cubic phase; ▽: cubic+H_{II}. Cubic phase was not observed in this work, and the existence of the cubic phase was ignored in the construction of the phase diagram. See text for explanation of the construction of e_2b line.

Uncertainty in determination of the coordinates of the specific points on the phase diagram is estimated to be within 3–5°C and 2–3 wt% of water. The major contribution to the composition uncertainty is from the extrapolation procedure. There are three sources of the temperature uncertainty: (i) the high heating rate (40°C/min) used for the DSC scans; (ii) the somewhat arbitrary choice of characteristic points on DSC peaks to represent phase transition temperatures; (iii) the sample-to-sample variations. There is also an uncertainty about the low-water content part of the phase diagram; the minor phase that coexists with the L_c phase in the low-water content part of the phase diagram was provisionally identified from the X-ray diffraction experiments as the L_β phase below 0°C and H_{II} phase above 0°C, and the corresponding part of the phase diagram was constructed based on this assumption. Lack of higher-order diffractions did not allow for certainty about identification of those phases.

References

[1] J.H. Crowe, L.M. Crow, in: G. Gregoriadis (Ed.), Liposome Technology, 2nd edn., vol. 1, CRC Press, Boca Raton, FL, 1993, pp. 229–252.
[2] P.L. Steponkus, M. Uemura, M.S. Webb, in: P.L. Steponkus (Ed.), Advances in Low-Temperature Biology, vol. 2, JAI Press, London, 1993, pp. 211–312.
[3] J.M. Seddon, G. Cevc, R.D. Kaye, D. Marsh, Biochemistry 23 (1984) 2634–2644.
[4] C. Grabielle-Madelmont, R. Perron, J. Colloid Interface Sci. 95 (1983) 471–482.
[5] B. Tenchov, Chem. Phys. Lipids 57 (1991) 165–177.
[6] D. Marsh, CRC Handbook of Lipid Bilayers, CRC Press, Boca Raton, FL, 1990.

[7] R. Koynova, J. Brankov, B. Tenchov, Eur. Biophys. J. 25 (1997) 261–274.
[8] M.S. Webb, S.W. Hui, P.L. Steponkus, Biochim. Biophys. Acta 1145 (1993) 93–104.
[9] M.S. Webb, T.C. Irving, P.L. Steponkus, Biochim. Biophys. Acta 1239 (1995) 226–238.
[10] M.S. Webb, T.C. Irving, P.L. Steponkus, Biochim. Biophys. Acta 1326 (1997) 225–235.
[11] K. Gawrisch, V.A. Parsegian, D.A. Hajduk, M.W. Tate, S.M. Gruner, N.L. Fuller, R.P. Rand, Biochemistry 31 (1992) 2856–2864.
[12] R.P. Rand, N.L. Fuller, S.M. Gruner, V.A. Parsegian, Biochemistry 29 (1990) 76–87.
[13] R.P. Rand, N.L. Fuller, Biophys. J. 66 (1994) 2127–2138.
[14] E. Shyamsunder, S.M. Gruner, M.W. Tate, D.C. Turner, P.T. So, C.P.S. Tilcock, Biochemistry 27 (1988) 2332–2336.
[15] M.M. Kozlov, S. Leikin, R.P. Rand, Biophys. J. 67 (1994) 1603–1611.
[16] W. Pohle, C. Selle, Chem. Phys. Lipids 82 (1996) 191–198.
[17] J. Wolfe, Z. Yan, J.M. Poe, Biophys. Chem. 49 (1994) 51–58.
[18] S. Glasstone, Textbook of Physical Chemistry, D. Van Nostrand, Princeton, NJ, 1946, pp. 669–670.
[19] R.C. Weast (Ed.), Handbook of Chemistry and Physics, 53rd edn., The Chemical Rubber Co., 1972–1973.
[20] L.B. Rokland, Anal. Chem. 32 (1960) 1375–1376.
[21] L. Greenspan, J. Res. Natl. Bureau Standards A Phys. Chem. 81A (1977) 89–96.
[22] Z.-W. Yu, W.P. Williams, P.J. Quinn, Arch. Biochem. Biophys. 332 (1996) 187–195.
[23] L.G. Dowell, S.W. Moline, A.P. Rinfert, Biochim. Biophys. Acta 59 (1962) 158–167.
[24] M.W. Tate, E. Shyamsunder, S.M. Gruner, K.L. D'Amico, Biochemistry 31 (1992) 1081–1092.
[25] P. Gordon, Principles of Phase Diagrams in Material Systems, McGraw-Hill, New York, 1968.
[26] V.L. Bronshteyn, P.L. Steponkus, Biophys. J. 65 (1993) 1853–1865.
[27] F. Franks, M.H. Asquith, C.C. Hammond, S.le B. Hellen, P. Echlin, J. Microsc. 110 (1977) 223–238.
[28] M. Caffrey, Biochemistry 24 (1985) 4826.
[29] R. Marinov, E.J. Duforc, Eur. Biophys. J. 24 (1996) 423–431.
[30] G. Bryant, J. Wolfe, Cryo-Letters 13 (1992) 23–36.
[31] J.M. Seddon, K. Harlos, D. Marsh, J. Biol. Chem. 258 (1983) 3850–3854.
[32] M.J. Ruocco, G.G. Shipley, Biochim. Biophys. Acta 691 (1982) 309–320.
[33] J.M. Seddon, K. Harlos, D. Marsh, J. Biol. Chem. 258 (1983) 3850–3854.
[34] B.G. Tenchov, A.I. Boyanov, R.D. Koynova, Biochemistry 23 (1984) 3553–3558.
[35] E.Y. Shalaev, P.L. Steponkus, Cryobiology 35 (1997) 338–339.
[36] R.P. Rand, N.L. Fuller, Biophys. J. 66 (1994) 2127–2138.
[37] J.T. Gleeson, E. Shyamsunder, S.M. Gruner, Biophys. J. 67 (1994) 706–712.
[38] I. Ueda, H.S. Tseng, Y. Kaminoh, S.-M. Ma, H. Kamaya, S.H. Lin, Mol. Pharmacol. 29 (1986) 582–588.
[39] C. Grabielle-Madelmont, R. Perron, J. Colloid Interface Sci. 95 (1983) 483–493.
[40] W.P. Williams, A.P.R. Brain, B.A. Cunningham, D.H. Wolfe, Biochim. Biophys. Acta 1326 (1997) 103–114.
[41] R. Koynova, M. Caffrey, Chem. Phys. Lipids 69 (1994) 1–34.
[42] R.M. Epand, Chem. Phys. Lipids 36 (1985) 387–393.

References referring to Supplementary materials

[S1] T. Hatakeyama, F.X. Quinn, Thermal Analysis. Fundamentals and Applications to Polymer Science, John Wiley and Sons, Chichester, 1994, p. 65.
[S2] S. Mabrey, J.M. Sturtevant, Proc. Natl. Acad. Sci. USA 73 (1976) 3862–3866.
[S3] H-n. Lin, S. Li, G. Wang, E.B. Brumbauh, C. Huang, Biochim. Biophys. Acta 1283 (1996) 199–206.
[S4] D. Bach, in: D. Chapman (Ed.), Biomembrane Structure and Functions, Verlag Chemie, Weinheim, 1984, p. 3.
[S5] G. Bryant, J.M. Pope, J. Wolfe, Eur. Biophys. J. 21 (1992) 223–232.
[S6] K. Gawrisch, V.A. Parsegian, D.A. Hajduk, M.W. Tate, S.M. Gruner, N.L. Fuller, R.P. Rand, Biochemistry 31 (1992) 2856–2864.
[S7] M.M. Kozlov, S. Leikin, R.P. Rand, Biophys. J. 67 (1994) 1603–1611.
[S8] M.W. Tate, E. Shyamsunder, S.M. Gruner, K.L. D'Amico, Biochemistry 31 (1992) 1081–1092.
[S9] C.G. Bergeron, S.H. Risbud, Introduction to Phase Equilibria in Ceramics, The American Ceramic Society, Columbus, OH, 1984.